

The multimeric structure of polycystin-2 (TRPP2): structural–functional correlates of homo- and hetero-multimers with TRPC1

Peng Zhang^{1,2}, Ying Luo⁴, Bernard Chasan⁵, Silvia González-Perrett³, Nicolás Montalbeti³, Gustavo A. Timpanaro³, María del Rocío Cantero³, Arnolt J. Ramos^{1,2}, Wolfgang H. Goldmann^{1,2,†}, Jing Zhou⁴ and Horacio F. Cantiello^{1,2,3,*}

¹Nephrology Division and Electrophysiology Core, Massachusetts General Hospital East, Charlestown, MA 02129, USA, ²Department of Medicine, Harvard Medical School, Boston, MA 02115, USA, ³Laboratorio de Canales Iónicos, ININCA, UBA-CONICET, Buenos Aires C1122AAJ, Argentina, ⁴Renal Division, Department of Medicine, Brigham's and Women's Hospital, Harvard Medical School, Boston, MA 02115, USA and ⁵Physics Department, Boston University, Boston, MA 02115, USA

Received November 10, 2008; Revised and Accepted January 12, 2009

Polycystin-2 (PC2, TRPP2), the gene product of *PKD2*, whose mutations cause autosomal dominant polycystic kidney disease (ADPKD), belongs to the superfamily of TRP channels. PC2 is a non-selective cation channel, with multiple subconductance states. In this report, we explored structural and functional properties of PC2 and whether the conductance substates represent monomeric contributions to the channel complex. A kinetic analysis of spontaneous channel currents of PC2 showed that four intrinsic, non-stochastic subconductance states, which followed a staircase behavior, were both pH- and voltage-dependent. To confirm the oligomeric contributions to PC2 channel function, heteromeric PC2/TRPC1 channel complexes were also functionally assessed by single channel current analysis. Low pH inhibited the PC2 currents in PC2 homomeric complexes, but failed to affect PC2 currents in PC2/TRPC1 heteromeric complexes. Amiloride, in contrast, abolished PC2 currents in both the homomeric PC2 complexes and the heteromeric PC2/TRPC1 complexes, thus PC2/TRPC1 complexes have distinct functional properties from the homomeric complexes. The topological features of the homomeric PC2-, TRPC1- and heteromeric PC2/TRPC1 channel complexes, assessed by atomic force microscopy, were consistent with structural tetramers. TRPC1 homomeric channels had different average diameter and protruding height when compared with the PC2 homomers. The contribution of individual monomers to the PC2/TRPC1 hetero-complexes was easily distinguishable. The data support tetrameric models of both the PC2 and TRPC1 channels, where the overall conductance of a particular channel will depend on the contribution of the various functional monomers in the complex.

INTRODUCTION

The gene product of *PKD2*, PC2, one of the genes implicated in ADPKD (1), belongs to the superfamily of TRP channels (2,3). PC2 (4) is a large conductance, Ca²⁺-permeable non-selective cation channel (5,6), which is involved in Ca²⁺ transport (5,7) and in Ca²⁺ signaling in renal epithelial cells (8). As most prototypical TRP channel proteins, PC2 is

topologically organized in six transmembrane (6TM) domains, and cytoplasmic carboxy- and amino-termini (1). This topology, which is shared by a number of K⁺ channels (9), is assembled such that a sensor region is expected in TMs 1–4, and a pore region, located in TMs 5–6, containing the P-loop. Based on their sequence similarities with the pore-forming α subunit of voltage-gated Ca²⁺ channels that contain

*To whom correspondence should be addressed at: Nephrology Division and Electrophysiology Core, Massachusetts General Hospital East, 149 13th Street, Charlestown, MA 02129, USA. Tel: +1 6177265640; Fax: +1 6177265669; Email: cantiello@helix.mgh.harvard.edu

†Present address: Center for Medical Physics and Technology, Friedrich Alexander University, Erlangen-Nuerenberg, Germany.

four intra-molecular 6TM domains (10), TRP channels are expected to assemble as homo- and/or hetero-multimers, particularly potential tetramers. Similar assemblies have been found for the *Shaker* type K⁺ channels (9) and cyclic nucleotide-gated (CNG) channels (11). Functional diversity by TRP channels is expected to lie in structural combinations of heterologous monomers. Hetero-multimerization by TRP channels was originally observed between *Drosophila* TRP and TRPL channels (12). The homo-tetrameric structure of the Ca²⁺-permeable TRP channels TRPV6 (13–16) and TRPC1 (17), for example, has been confirmed. Several 6TM containing voltage-gated and ligand-gated channels are also tetramers (14,15,18–20). Interestingly, the multimeric composition of a particular channel may correlate with its functional properties, including those reflected in the presence of functional subconductance states. The tetrameric glutamate receptor, for example, displays subconductance states, which are correlated with the subunit composition of the channel complex (20). Heteromeric assembly of TRP channels, including PC2 (21) may provide functional and regulatory diversity among channel complexes (12,22,23). PC2 is known to interact with TRPC1 (24), providing distinct functional properties to the channel complex (25). The PC2 channel often displays identical subconductance levels (32 pS) (5), representing an intrinsic property of PC2, as both endogenous PC2 from plasma membrane, and the *in vitro* transcribed/translated gene product, display similar functional features. Here, we determined that the conductive substates in PC2 and PC2/TRPC1 multimers are consistent with the individual contribution of monomers to the channel complex. Further, the formation of PC2/TRPC1 hetero-complexes renders distinct functional properties, such as resistance to low pH, only observed in TRPC1 homo-complexes, but not PC2 complexes. The topological structure of these channel complexes was confirmed by atomic force microscopy (AFM), which showed that PC2 and TRPC1 homomers, as well as PC2/TRPC1 heteromers, assemble as structural tetramers. Functional diversity in both PC2 and TRPC1 may represent the individual ratio of the particular monomers composing the channel complex.

RESULTS

Presence of subconductance states in PC2

Wild-type PC2 single channel currents (Fig. 1) often display, spontaneous, short closures into either one of the four most common subconductance states of identical amplitude (~32 pS, Fig. 1A–D) as originally reported (5). This is observed in the endogenous PC2 (Fig. 1A–C) from human syncytiotrophoblast (hST) and the *in vitro* translated gene product (Fig. 1D), indicating an intrinsic property of the PC2 channel. Upon full closure from its maximal conductance state, PC2 often re-opens in a staircase fashion, ‘climbing up’ the increasing conductance levels, from previous conductance states (Fig. 1D). This phenomenon is both voltage- and pH-dependent (Fig. 1E and F). An average of such spontaneous sojourns ($n = 9$, from five experiments, Fig. 1E and F) shows a voltage-dependent staircase increase in conductance. Channel openings at 0 mV showed discrete (~3.8 ms) semi-conductance delays not detected at 40 mV ($P < 0.02$, $n = 7$).

Voltage dependence of the activation process also follows from voltage inactivation as recently reported (26) (data not shown). The lifetime of each occupancy state can also be modified by ‘protonation’ of the channel (26) (Fig. 1F). This pH effect was also voltage-dependent (Fig. 1F), suggesting that the protonation effect itself is voltage-dependent. The simplest interpretation of the data is consistent with the hypothesis that PC2 is a functional tetramer, whose conductance levels correspond to the sequential ‘staircase’ activation of each one of the four ‘monomeric’ units. According to this view, a fully functional channel requires four subunits necessary for a complete channel opening. To confirm this view, the quaternary structure of the PC2 channel was determined by western blot analysis after gel electrophoresis of affinity purified PC2 under both denaturing (Fig. 1G, Left, with SDS present) and non-denaturing (Fig. 1G, Right, without SDS) conditions. Large, 440 kDa (tetramers) and higher molecular weight complexes were preserved under non-denaturing conditions (Fig. 1G, Right), when compared with 110 kDa monomers under denaturing conditions (Fig. 1G, Left). Interestingly, 210 kDa complexes were also observed under denaturing condition (Fig. 1G, Left), which are most consistent with highly stable dimeric structures. An additional ~70 kDa band was detected under denaturing conditions, which is in agreement with previous reports by us and others using different antibodies (27–30). This suggests that the smaller band could be a degraded (cleaved?) form of PC2 but not due to the non-specific recognition of the antibody.

Electrophysiological features of TRPC1 and TRPC1/PC2 complexes

To disclose the individual contribution of the various monomers in PC2 to the single channel conductance of the complex, we explored replacing PC2 subunits with TRPC1 monomers. The electrical properties of the TRPC1 channel were first determined in the homomeric complex. Reconstituted TRPC1 displayed a single channel conductance of 5.0 ± 0.7 pS ($n = 5$) in the presence of a KCl chemical gradient (Fig. 2A and B, 150 versus 15 mM K⁺ for *cis*- and *trans*-chambers, respectively). TRPC1 channels also displayed a 22.8 ± 2.0 pS ($n = 5$) conductance (Fig. 2B), consistent with a functional tetramer. The TRPC1 tetramer showed on occasion four subconductance states (Fig. 2C and D), consistent with four units of the 5 pS small channel shown in Fig. 2B. Two features, which contrast with those previously observed with the PC2 channel (5,26), included the fact that the TRPC1 homomeric channels were insensitive to both amiloride (200 μ M, *trans* side, $n = 10$, Fig. 2E) and low cytoplasmic pH (6.4–5.9, *cis* side, $n = 7$, Fig. 2F). Owing to these functional differences, TRPC1/PC2 channel monomers were mixed and reconstituted at equimolar ratios (1:1, w:w) in a lipid bilayer reconstitution chamber (Figs 3–5). The electrophysiological properties of the PC2/TRPC1 hetero-complexes were quite distinct, and different from any of the homo-complexes of either type (Figs 1 and 2). PC2-mediated single-channel deflections were easily identifiable by their large conductance compared with the smaller TRPC1 (~5 versus 32 pS, respectively, Fig. 3). In most experiments

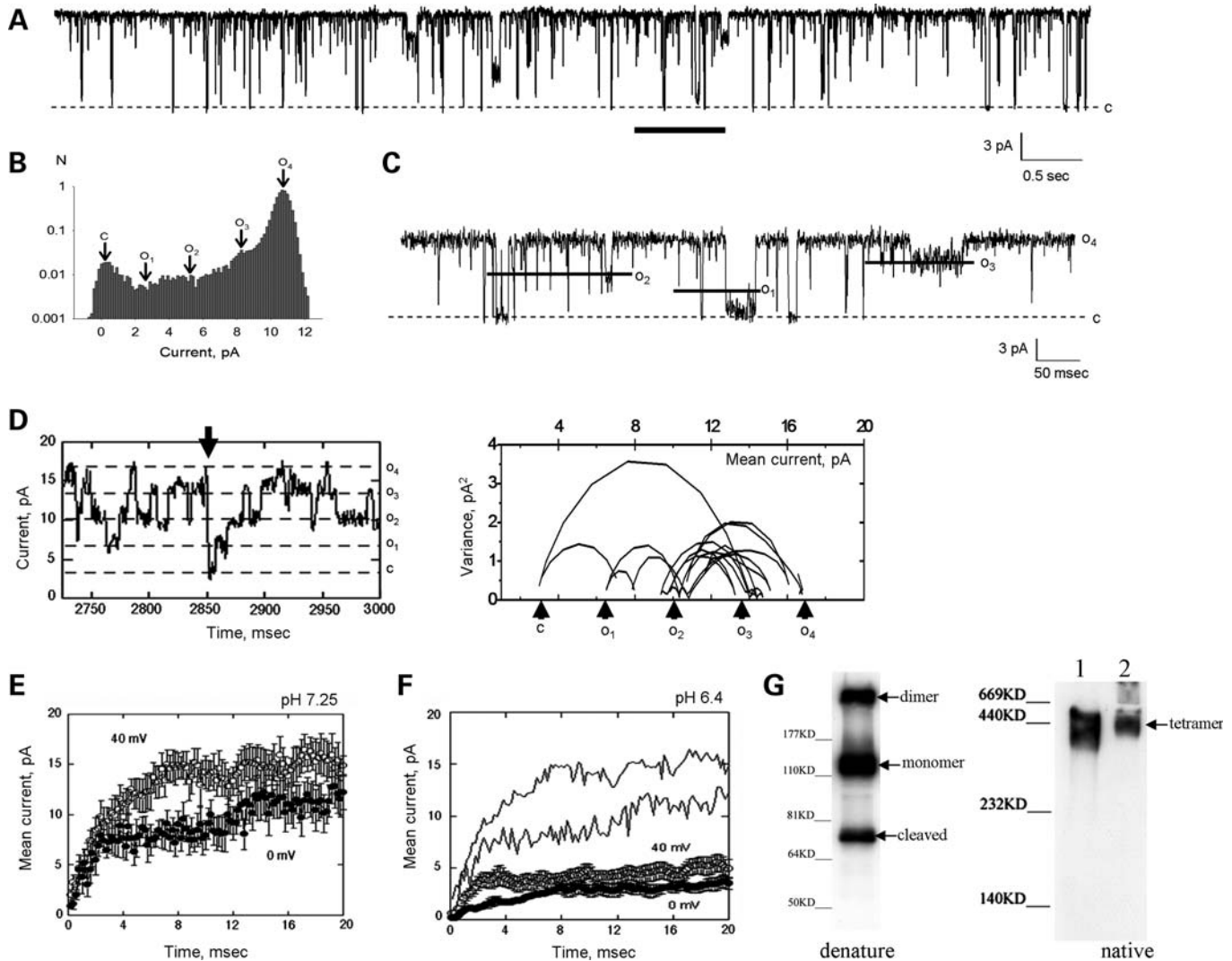


Figure 1. Presence of subconductance states in the PC2 channel. (A) Single-channel currents of endogenous hST PC2. Holding potential is 60 mV in asymmetric K^+ . (B) Three intermediate subconductance levels are identifiable in the all-point histogram. C, closing state; O_1 – O_4 , four sub-conductance states. (C) Expanded single-channel current subconductance states of PC2 from region indicated with horizontal line in (A). (D) Examples of subconductance states in the purified PC2 reconstituted protein as in (26). Spontaneous, full channel closures (arrow) are followed by ‘staircase’ activation of the four subconductance states, revealing four identical functional subunits (dashed lines). This is further evidenced by the mean versus variance analysis of the tracing (Right). (E) The mean activation was calculated by averaging kinetics after full closures. Voltage-dependence of subconductance states (open circles, 40 mV, compared with filled symbols, 0 mV, $P < 0.02$). Data are the average of nine and seven sojourns, from five experiments, respectively. Averages do not display discrete steps, indicating the variable time spent by the channel at each subconductance level. There is a kinetic delay only observed at 0 mV. (F) Spontaneous subconductance states in PC2 (Top, dashed lines) can be further modified by reduction in cytoplasmic pH (*cis* chamber), which decreases PC2 channel activity as previously reported (26). Solid lines indicate the respective averages at normal pH (7.25, also see E). (G) The quaternary structure of PC2 was confirmed by gel electrophoresis of affinity purified PC2 under denaturing (Left) and non-denaturing (Right) conditions. The presence of 440 kDa protein complexes (tetramers) were observed under non-denaturing conditions, in contrast to denaturing conditions, which only showed monomers (~110 kDa), dimers (~210 kDa) and a cleaved form of PC2 (~70 kDa). Lane 1 indicates purified protein and lane 2 the whole cell lysate in the native gel (Right).

(Figs 4 and 5), the deflections also showed striking differences, including much higher open probability for the TRPC1 contribution, while fast flickering of the open state in the PC2 components of the channel. The single-channel conductance of the PC2/TRPC1 hetero-complex (Fig. 3D and E) was intermediate between the conductances of PC2 (26) and TRPC1 homomers (Fig. 2B). Most interestingly, the data of single channel current deflections at various voltages suggest that a subpopulation of PC2/TRPC1 channel complexes behaved, in average, as TRPC1 homomers. In Figure 3D, the blue line and triangles

are the fitted data to a subpopulation of TRPC1/PC2 complexes, whereas the green line shows the fitted I–V relationship for TRPC1 homomers as shown in Figure 2B. The conductance of this subpopulation of TRPC1/PC2 complexes was very close to that of TRPC1 homomers. The remainder TRPC1/PC2 complexes had a single-channel conductance of 55.8 ± 2.9 pS ($n = 22$, Fig. 3D, red lines and circles), which is only 35% of that observed for the PC2 homomer (Fig. 3D, grey line, 157 ± 4.9 , $n = 7$, $P < 0.001$, d.f. = 27). This conductance is, however, 245% higher than that of

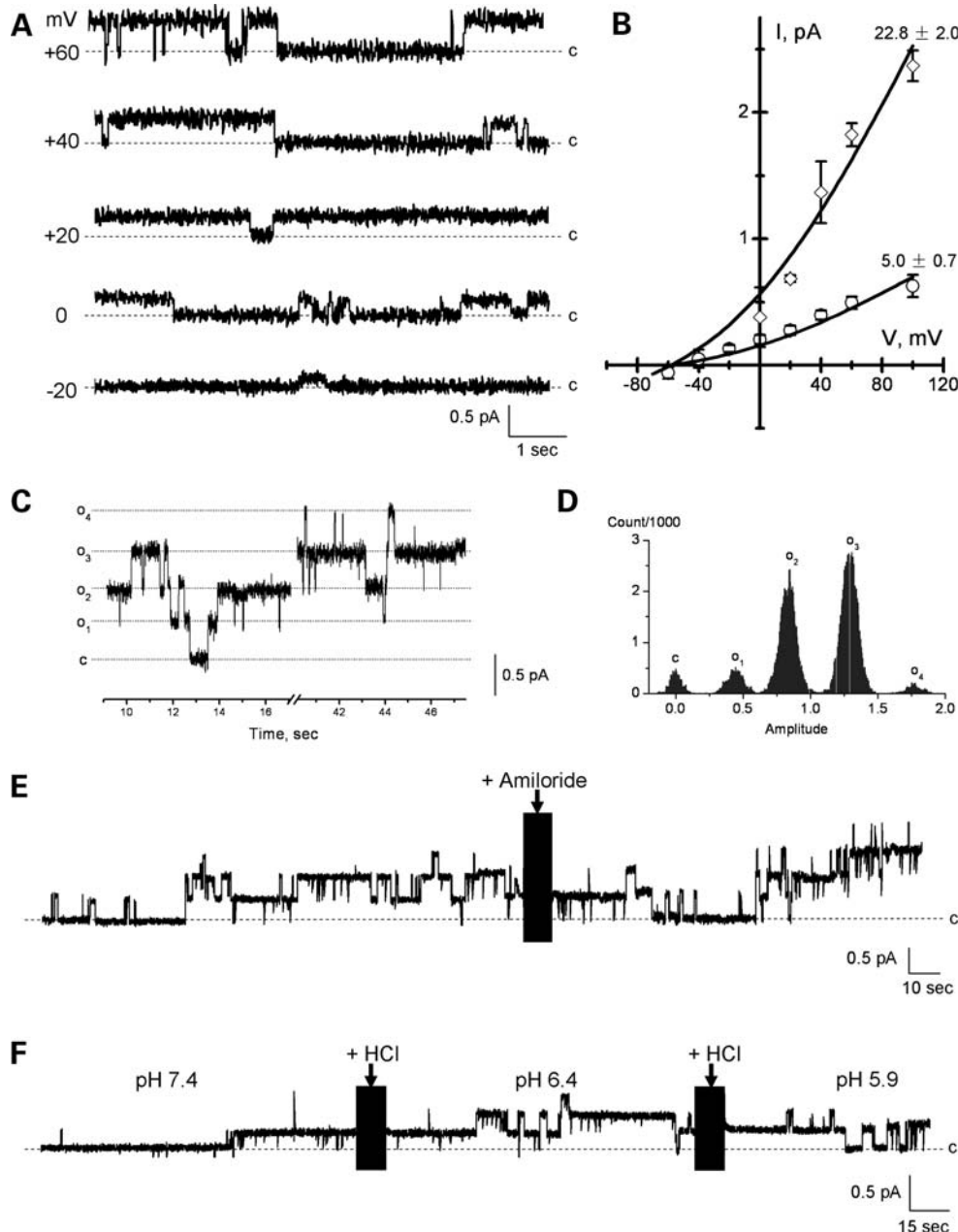


Figure 2. Electrophysiology of the TRPC1 channel. (A) Single-channel currents of affinity-purified TRPC1 at different holding potentials in asymmetrical K^+ . (B) Current-to-voltage relationship for the TRPC1, indicating a single-channel conductance of 5.0 ± 0.7 pS ($n = 5$), and a bigger conductance of 22.8 ± 2.0 pS ($n = 5$). (C) Representative tracing showing a TRPC1 channel complex displays four subconductance states at +100 mV. (D) All-point histogram of (C) shows the presence of four subconductance states in TRPC1. (E) Effect of amiloride (200 μ M, *trans* side) on TRPC1 single-channel currents. Addition of amiloride to the *trans* chamber was without the effect on the purified channel. Representative tracings from $n = 10$. (F) Lowering the cytoplasmic pH had no effect on the TRPC1 single-channel currents. The cytoplasmic pH was reduced by addition of 1.0 N HCl to the *cis* chamber. Data representative of $n = 7$ experiments.

TRPC1 alone (Fig. 3D, green line, 22.8 ± 2.0 pS, $n = 5$, $P < 0.001$, d.f. = 25). There is also a voltage-dependent shift in conductance at higher potentials (+60 to +150 mV in the reconstitution setup), such that the complex has a conductance of 53.7 ± 4.8 pS ($n = 7$, Fig. 3D, red linear line), while the extrapolated conductance for the same complex at those same potentials would be 122 pS. This would suggest that the TRPC1 contribution to the channel may close at higher potentials, to let the PC2 components of the channel prevail

(Fig. 3D, the red linear line at higher potentials). The distinct contribution of either component further defined by addition of either amiloride (200 μ M, *trans* side, Fig. 4) or 1.0 N HCl (*cis* side, Fig. 5) to lower the pH to 5.9 was used to modify the single-channel currents of PC2 subunits in the functional hetero-complex. Interestingly, while amiloride addition blocked the PC2, but not the TRPC1 contribution to the PC2/TRPC1 complex (Fig. 4, $n = 7$), lowering the pH was without effect on the overall hetero-complex conductance

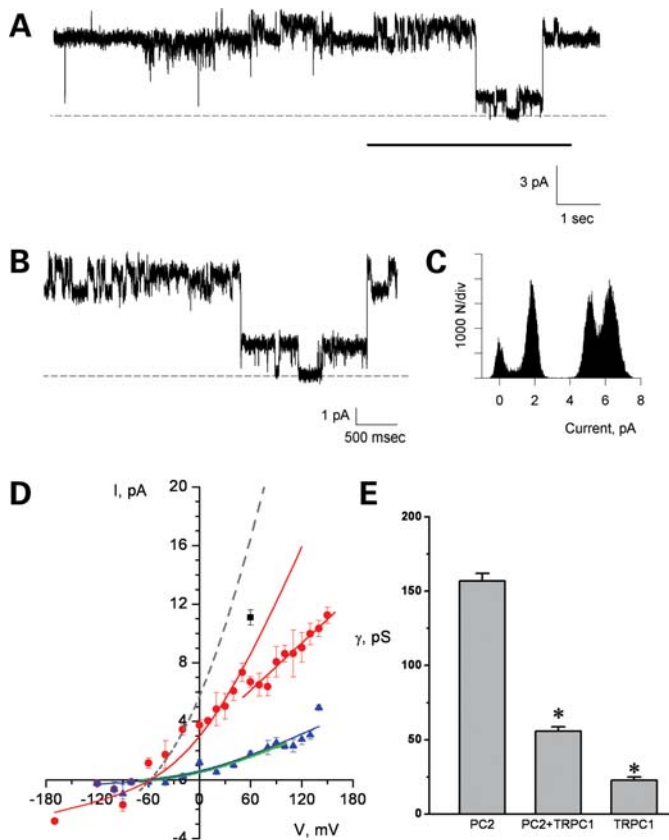


Figure 3. Electrophysiological features of the PC2/TRPC1 hetero-complex. PC2/TRPC1 hetero-complex displayed two conductances (A and B), which correspond to the smaller TRPC1 and bigger PC2 channels. (C) Shows the all point histogram of the extended tracing (B). (D) The I–V relationship of PC2/TRPC1 hetero-complex shows a conductance (red lines and circle) between those of homomeric PC2 (157 pS, higher grey dashed line) (26) and homomeric TRPC1 (~23 pS, lower green line indicates the fitted I–V relationship for TRPC1 homomers as shown in (Fig. 2B)). There is also a lower conductance present in the PC2/TRPC1 hetero-complexes (the blue triangles and line), which is close to the conductance of homomeric TRPC1. The black square represents PC2/TRPC1 complexes showing a higher conductance, closer to PC2 contribution alone. (E) The bar graph for the conductance of PC2, TRPC1 and PC2/TRPC1 complexes indicates that the single-channel conductance of the heterocomplex is statistically different from either homomer alone. * indicates $P < 0.001$.

(Fig. 5, $n = 7$). This evidence indicates that while the PC2/TRPC1 channel contains functional units of each contributing protein, the presence of TRPC1 in the hetero-complex renders the contributing PC2 refractory to low pH.

Topology of the PC2 and TRPC1 homomeric complexes

To identify the topological structure of the PC2/TRPC1 channels, the affinity-purified proteins were inserted into liposomes as for the electrophysiological studies. The reconstituted proteins were then imaged in solution by scanning flattened PC2-containing liposomes onto freshly cleaved mica with an atomic force microscope (Fig. 6). The topological structure of the PC2 channel showed the contribution of four monomers (Fig. 6A–C). PC2 channels were identified as bell-shaped structures with a 135 ± 3.38 nm diameter ($n = 107$, mean \pm SEM), and an average height of 1.21 ± 0.05 nm ($n = 107$, Fig. 6D). A

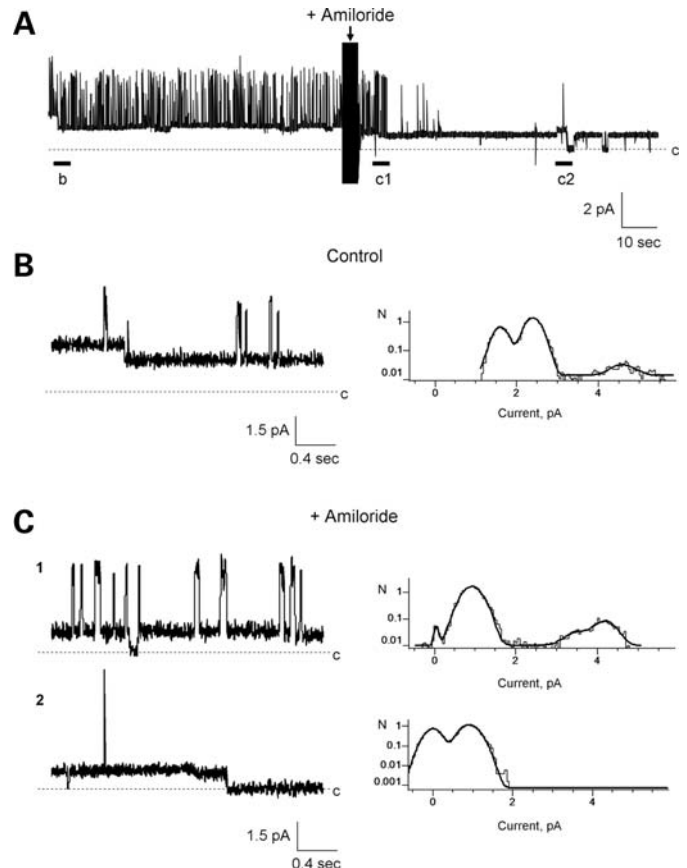


Figure 4. Electrophysiological features of the PC2/TRPC1 hetero-complex. Effect of amiloride. (A) Single-channel currents of reconstituted PC2/TRPC1 channel complexes in asymmetrical K^+ . Note the flickering in the large conductance deflections, consistent with PC2 contribution, contrasting the much longer open probability of the small conductance states observed in the TRPC1 channel contribution to the complex. (B) Expanded single-channel currents unmask the large conductance PC2, and smaller conductance TRPC1 under control conditions. (C) PC2 conductance was blocked by amiloride but TRPC1 conductance persisted. All-point histograms to the right of the panels indicate the channel conductances under each condition. Data are representative of $n = 7$ independent experiments.

distribution of the diameter population (Fig. 6E) was consistent with a sharp peak at 116 ± 1.9 nm ($n = 61$, the most likely monomeric contributor to the tetramer), and a wider, larger population of 163 ± 2.0 nm ($n = 46$). The height showed a trimodal population with means of 0.73 ± 0.01 nm ($n = 43$), and a higher population at 1.23 ± 0.01 nm ($n = 46$). A few instances of approximately 1.81 ± 0.02 nm heights ($n = 18$) were also observed, which are consistent with channel proteins bound to, but not inserted in the lipid bilayer. The PC2 monomers in the homomeric channel complexes were further identified by exposure to an anti-PC2 antibody (Catalog no. 52-5217, Zymed, South San Francisco, CA, USA), which increased both the height and diameter of the complex (Fig. 7). Conversely, a decrease of the sample's pH by addition of HCl modified the topology of the PC2 channel complex, such that the different PC2 complexes had a reduced diameter compared with controls (Fig. 8). The calculated volume of the PC2 homomeric channel was 3663 ± 139 nm³ ($n = 97$). This value was the peak obtained from a population analysis

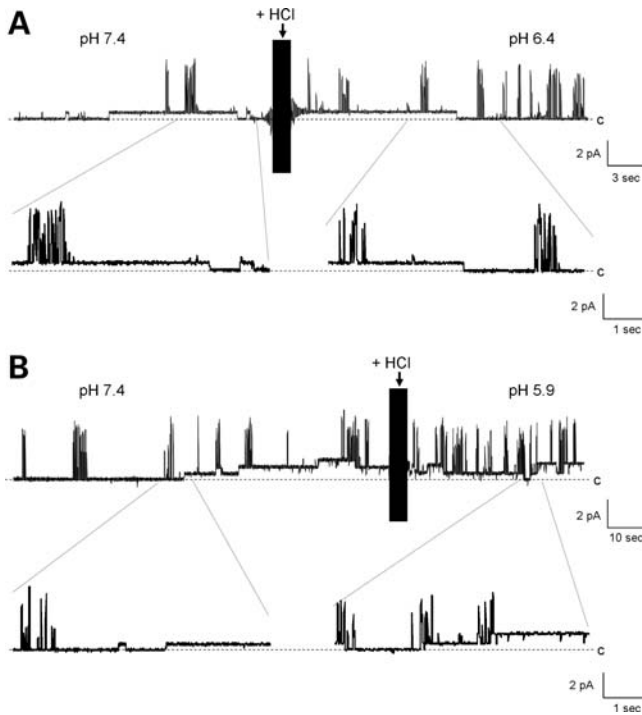


Figure 5. Electrophysiological features of the PC2/TRPC1 hetero-complex. Effect of lowering pH. The PC2/TRPC1 hetero-complexes were insensitive to changes in pH (*cis* chamber). Data were obtained in the presence of KCl chemical gradient. Lowering the pH to either 6.4 (A) or 5.9 (B) had no effect on the channel activity of PC2/TRPC1 hetero-complexes. Data are representative of $n = 7$.

of molecular volumes (Fig. 10A and B) calculated for heights lower than 2 nm. The weak linear correlation for the height versus diameter (Fig. 10A) indicates that the complexes evaluated for measurement were inserted and not apposed to the membrane. The distribution of the population indicates step-growth-type polymerization of higher molecular weight complexes as well.

The topological structure of the homomeric TRPC1 channel was also determined by AFM imaging of affinity purified, reconstituted protein, which was carried out by scanning flattened TRPC1-containing liposomes onto freshly cleaved mica in the solution (Fig. 9). TRPC1 channels were identified as multi-lobular structures with an average diameter of 49.3 ± 1.5 nm ($n = 105$, mean \pm SEM), and an average height of 3.1 ± 0.1 nm ($n = 105$) (Fig. 9D). A distribution of the diameter population was consistent with a sharp peak at 32.3 ± 0.7 nm ($n = 37$), and a wider, larger population of 51.6 ± 1.5 nm ($n = 68$) (Fig. 9E). The height also showed a multimodal population with means of 2.1 ± 0.1 nm ($n = 53$) and 3.6 ± 0.04 nm ($n = 41$) (Fig. 9F). A few instances of approximately 5.8 nm heights ($n = 11$) were also observed, which are consistent with channel proteins bound but not inserted in the lipid bilayer (Fig. 9F). The topology of the TRPC1 channel was consistent with a tetrameric complex (Fig. 9B and C). The calculated volume for the TRPC1 channel complex (Fig. 10C and D) was 1053 ± 51 nm³ ($n = 94$), remarkably different from that observed for the PC2 channel. The same criteria were used for data analysis

of TRPC1 complexes. However, excluded heights for volume calculations were higher than 5 nm.

Topology of the PC2/TRPC1 hetero-complexes

To identify the topological structure of the PC2/TRPC1 hetero-complexes, affinity purified PC2 was mixed in a 1:1 ratio with affinity purified TRPC1, in identical mixture to that previously tested in the electrophysiological studies. PC2/TRPC1 channel complexes were incorporated into liposomes of same lipid composition used in the lipid bilayer studies. The reconstituted channel complexes were imaged in solution by scanning flattened PC2/TRPC1-containing liposomes onto freshly cleaved mica (Fig. 11). PC2/TRPC1 complexes were identified as lax, asymmetrical structures (Fig. 11A and B), where both the PC2 and TRPC1 monomers could be identified by height in the channel complexes. Consistent with the mixing ratio, most channel complexes had a tetrameric topology, with two PC2 monomers, and two TRPC1 monomers in each (Fig. 11B and C, circles). TRPC1 homo-complexes (squares) and PC2 homo-complexes (hexagons) could also be identified (Fig. 11B). The 2:2 PC2/TRPC1 hetero-complexes had, in average, an overall diameter of 129 ± 3.6 nm ($n = 12$), which is between that of the homomeric PC2 complexes (163 ± 2.0 nm, Fig. 6E) and homomeric TRPC1 complexes (51.6 ± 1.5 nm, Fig. 9E). The contributing monomeric PC2 and TRPC1 in the hetero-complexes showed different height as expected (Fig. 11C), but their monomeric diameters were indistinguishable from each other, which were 43.7 ± 2.71 nm ($n = 9$) versus 45.3 ± 2.07 nm ($n = 9$), respectively (Fig. 11C). Interestingly, the PC2 monomeric diameter in the PC2/TRPC1 hetero-complexes was greatly decreased when compared with that in the PC2 homo-complexes, suggesting that interaction between molecules (PC2–PC2 and PC2–TRPC1) may greatly affect their topological dimension outside the membrane, which, however, needs further studies to confirm.

DISCUSSION

The members of the TRP superfamily of cation channels play diverse physiological roles, including receptor- and store-operated Ca²⁺ entry, mineral absorption, cell death and particularly as sensors for pain, heat, cold, sound, stretch, osmotic changes, etc. The wide variety of physiological functions, in which TRP channels are implicated, underscores diversity in structural and regulatory features. Despite heavily conserved transmembrane domains, the cytoplasmic domains of TRP channels are notably different, which are the target of different gating and regulatory mechanisms (2,3). Functional diversity by TRP family members also lies in the ability to hetero-oligomerize, thus creating a wider spectrum of TRP channel phenotypes. Although expected to be tetrameric structures, structural–functional evidence is only beginning to emerge (31). Moreover, the contribution of each monomeric unit to the functional channel complex is still largely unknown. In the present report, we demonstrated that PC2, TRPC1 and PC2/TRPC1 channel complexes are distinct units consistent with structural tetramers, which functionally correlate with the presence of subconductance states. This is in agreement with our original finding indicating that

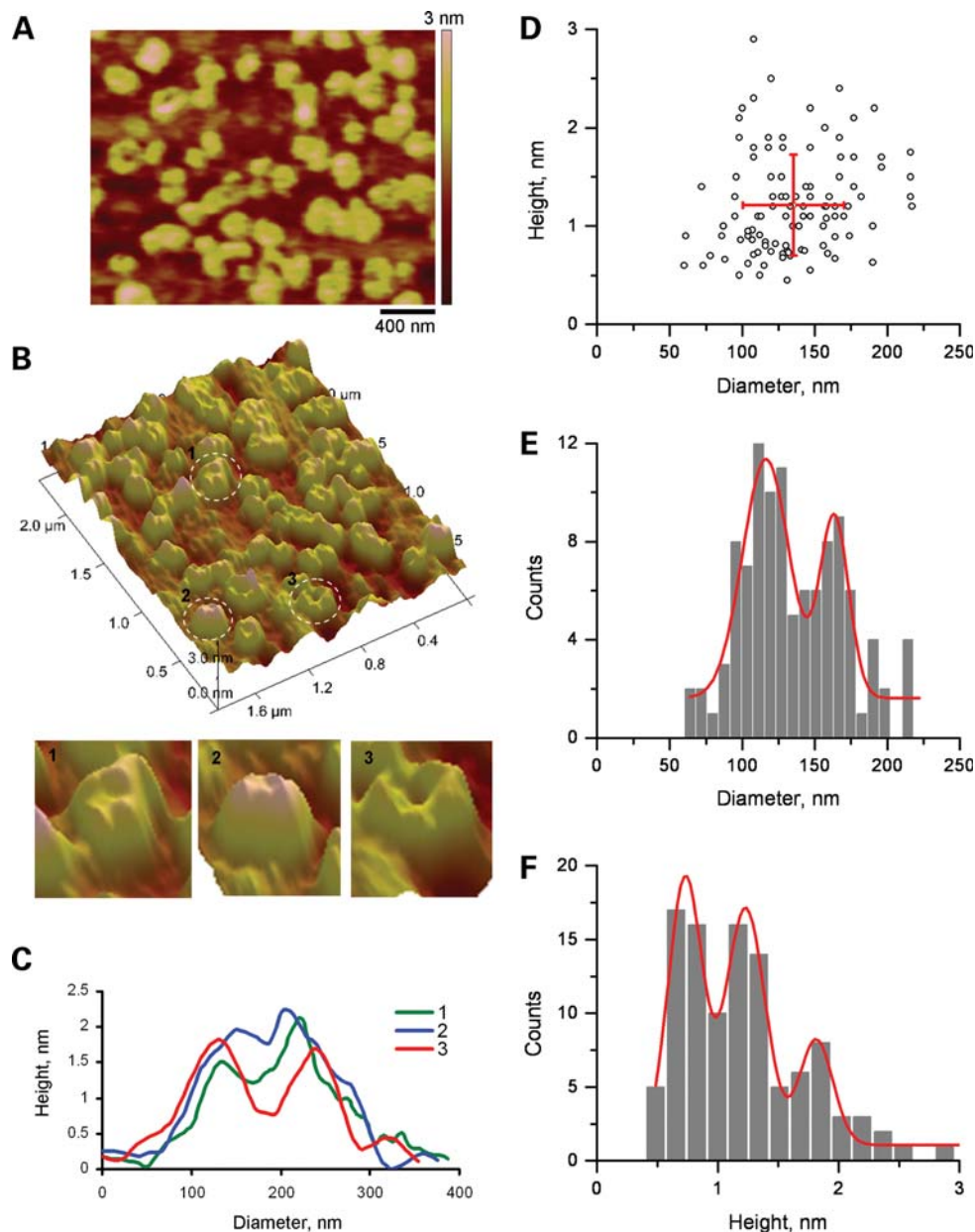


Figure 6. AFM imaging of PC2. (A) PC2 was imaged in flattened, PC2-containing proteoliposomes, onto freshly cleaved mica in saline solution. (B) Upper panel, PC2 channels were identified in AFM scans as round structures, often displaying a central indentation, and a tetra-lobular structure. Lower panel (1–3) showed three expanded PC2 structures highlighted in the circles on the upper panel. (C) Cross-section histograms from B1 – B3 indicate the height and diameter of the contributing monomers, and the central indentation. Three such measurements are superimposed in the graph. (D) Population analysis of channel units indicates that the monomers segregated in a scattered population ($n = 107$). (E) Analysis of the distribution of diameters indicates two peaks, suggesting asymmetry in the shape of the channels. (F) Further analysis of the distribution of heights indicates three peaks.

PC2 contains intrinsic subconductance states, whose resident times, can be modulated by changes in either cytoplasmic pH or holding potential (26). The presence of subconductance states has also been unmasked by functional inhibition with blocking agents such as amiloride, La^{3+} and anti-PC2 antibodies (5). The question we posed in the present study was as to whether each one of the four subconductance states in PC2 has a structural correlation in its monomeric components.

The topology of PC2 and TRPC1 channels was assessed by AFM imaging of lipid bilayer imbedded complexes in solution, thus, providing the first direct comparison between

structural and functional correlates of each channel complex. Although many channels are structural tetramers, the evidence for the putative tetrameric conformation of PC2 was heretofore lacking. The correlation between the AFM imaging and the single-channel currents indicates that each isolated monomer usually does not behave as a small conductance channel, but rather that at least four monomers of either protein (PC2 or TRPC1) are required to build a fully functional channel. The time residence and overall conductance at each substate are, therefore, a reflection of the number of contributing units to this tetrameric channel complex. The

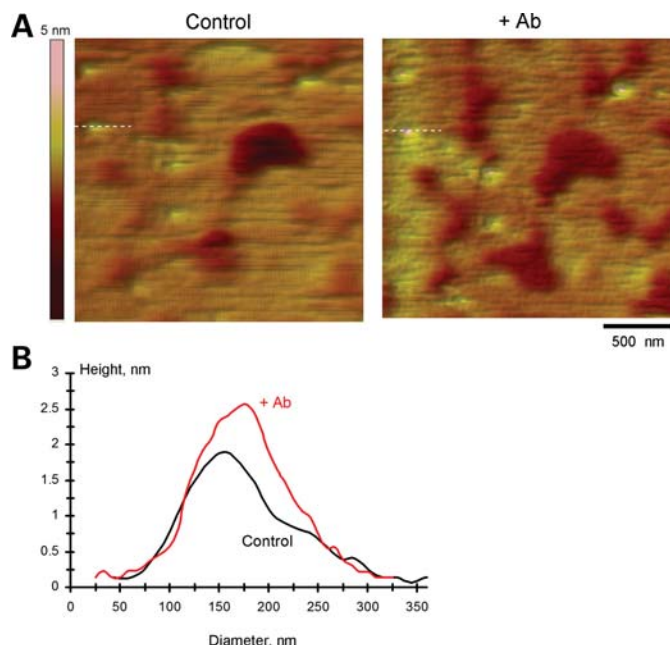


Figure 7. Effect of anti-PC2 antibody on AFM imaging of PC2. (A) PC2 monomers were identified in AFM scans (Scale bar, 500 nm) as round structures and the exposure to the anti-PC2 antibody (Zymed Catalog No. 52-5217) increased both the height and the diameter of PC2. (B) The cross sections at the lines indicated in (A) show the binding of PC2 antibody increased the apparent diameter and the height of PC2. Data are representative of two-paired experiments.

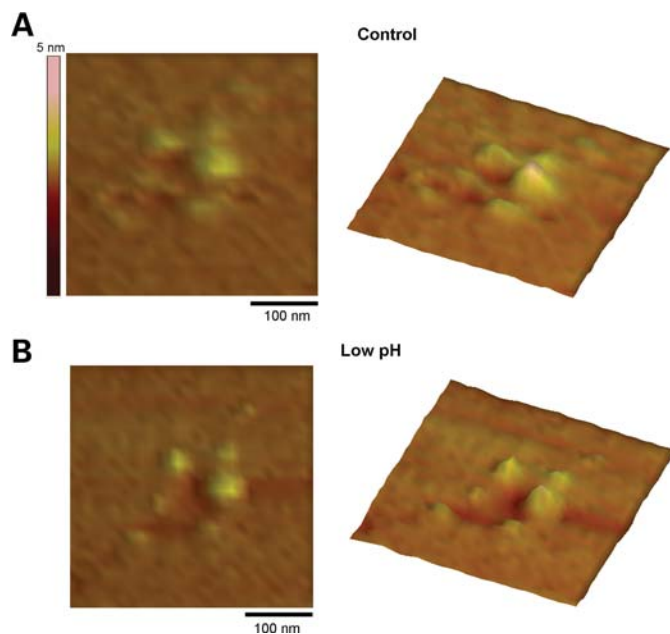


Figure 8. Changes in AFM imaging of PC2 at low pH. (A) PC2 was imaged in flattened, PC2-containing proteoliposomes, onto freshly cleaved mica in saline solution (pH 7.4). (B) Lowering the sample's pH (~6.1) decreased PC2's extra-membrane size. Data are representative of three-paired experiments.

lack of evidence for isolated 'monomeric' (small) channel conductances of PC2 in our preparations supports this contention. Full or partial PC2 channel inhibition by protonation at different pH suggests that in its fully closed state, the four

channel subunits are protonated (26), which can then become sequentially functional, as each one changes conformation. This particular change in conformation is likely to be hindered in the presence of one or more TRPC1 subunits in the complex.

Distinct oligomerization, or 'aggregation' domains (AD) (14) have been identified in the TRP superfamily members, including TRPC, TRPV, TRPM (32,33) and even TRPP (PC2) (24). Both the carboxy- and the amino-termini domains of TRP channels have been implicated in these interactions (34,35). These include the so-called TRP domain in the carboxy terminus (32), and the ankyrin domains found in the amino terminus region of several TRP channels. It is interesting to note, however, that neither one of these domains is present in PC2. Original work by Tsiokas *et al.* (24), demonstrated that structural interactions between PC2 and TRPC1 also emanate from the transmembrane domains in PC2, which might be implicated in the aggregation of the hetero-complex. These putative association domains may also have functional correlates. Our findings contend that specific aggregation regions in the monomers of the channel, once oligomerized into a functional complex, can be regulated by protonation, which plays both structural and functional roles by modifying the overall topological and conductive properties of the complex. Protonation in PC2, which we previously identified within the pore and is only reachable from the cytosolic side of the channel (26), likely helps screen charges and in turn allows conformational changes in the pore structure of the functional complex.

The tetrameric topology of PC2 and TRPC1 found in the current study is consistent with other channels, including the α_E subunit of the Ca^{2+} channel (1) and other TRP channels (13–16). However, stoichiometries other than tetramer were also observed for PC2 with both AFM imaging and Western blot analysis. Similar findings have been reported in TRPV6 (15). FRET analysis of TRP channels further suggests a loosely packed tetramer (13), which may depend on the aggregation structure of the channel complex. Thus, although our data support a tetramer as the most plausible PC2 functional topology, they do not exclude other topological structures. In light of the present findings, the expectation is that the non-tetrameric TRP channel with either fewer or more interacting subunits, would display, accordingly, different channel conductance and subconductance states. The ubiquitous distribution of TRP channels, including PC2 and TRPC1, and their ability to interact with each other (21,24) may underlie their relevance and functional diversity in cell signaling. Our evidence indicates that the presence of at least one, most likely two TRPC1 monomers in the PC2/TRPC1 channel complex, elicits dramatic changes in the single-channel conductance, open probability and responses to pH and amiloride. This, in itself, indicates that the stoichiometric contribution of a particular channel has to be ascertained before any conclusions can be drawn, when assessing TRP-mediated whole-cell currents, or heterologous systems where more than one particular TRP channel is expected.

Our results are in agreement with recent literature, indicating that the isolated proteins have a somewhat similar behavior to cell expression systems. The single-channel conductance of the tetrameric TRPC1 yielded a conductance of 22.8 pS, and a monomeric contribution of approximately 5 pS. This is slightly larger, but in agreement with recently reported data

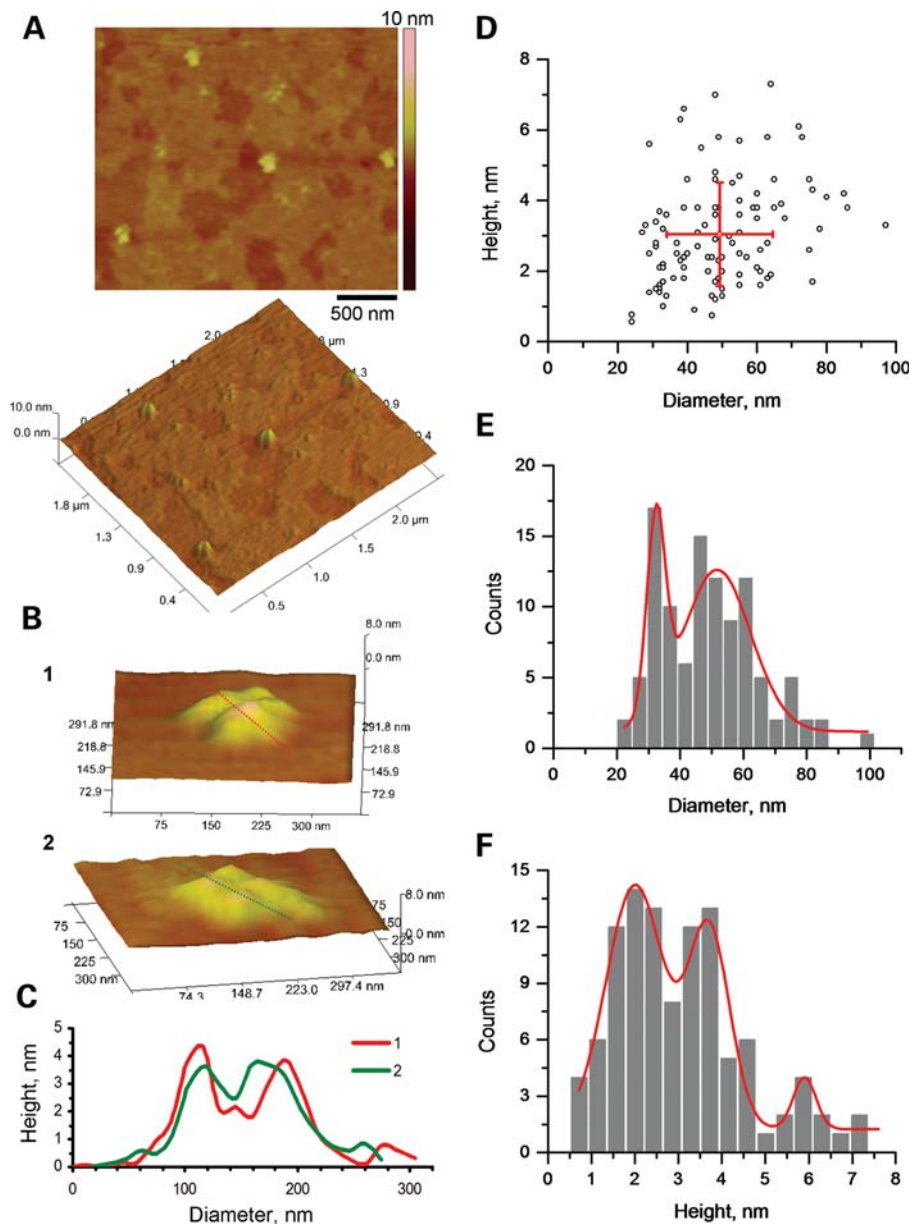


Figure 9. AFM imaging of TRPC1. (A) TRPC1 channels were identified in AFM scans (Scale bar, 500 nm) from flattened, TRPC1-containing proteoliposomes, placed onto freshly cleaved mica in saline solution as tetra-lobular structures as shown in the panel at the bottom. (B) The tetrameric structure can be easily distinguished in higher magnification scans (B panels 1,2). (C) Cross-section histograms from dashed lines in (B) indicate the height and diameter of the contributing monomers, and the central indentation. Two such measurements are superimposed (B panels 1,2) in the graph. (D) Population analysis of channel units indicates the average diameter and height, respectively ($n = 105$). (E) Analysis of the distribution of diameters indicates two peaks, suggesting asymmetry in the shape of the channels. (F) Further analysis of the distribution of heights indicates three peaks.

by Du *et al.* (36), who showed that TRPC1 in glomerular mesangial cells has a single-channel conductance of 17.2 pS. Bai *et al.* (25) reported a TRPC1 conductance of 16 pS. It is important to note, however, that these were patch clamping studies in the biological membrane, where the channel complex may be affected by the associated proteins or structural lipids. Considering the technical and experimental differences, however, it can be accepted as in close agreement. Our data indicate that the interaction between TRPC1 and PC2 in a channel complex modifies the functional properties expected for each one alone. The single-channel conductance of the

PC2/TRPC1 hetero-complexes was lower than PC2 homomers but higher than TRPC1 homomers, which is also in agreement with the results obtained by Bai *et al.* (25). Moreover, Bai *et al.* showed that TRPC1 was significantly activated by addition of the M1 muscarinic agonist oxotremorine-M (Oxo-M) in mIMCD3 cells, but was almost unresponsive to amiloride, a finding similar to ours for the isolated TRPC1 channel. They also demonstrated that co-transfection of PC2 with TRPC1 resulted in the formation of a channel with higher Ca^{2+} permeability, comparing to either channels alone, which confirms that TRPC1 and PC2 functionally interact to form an

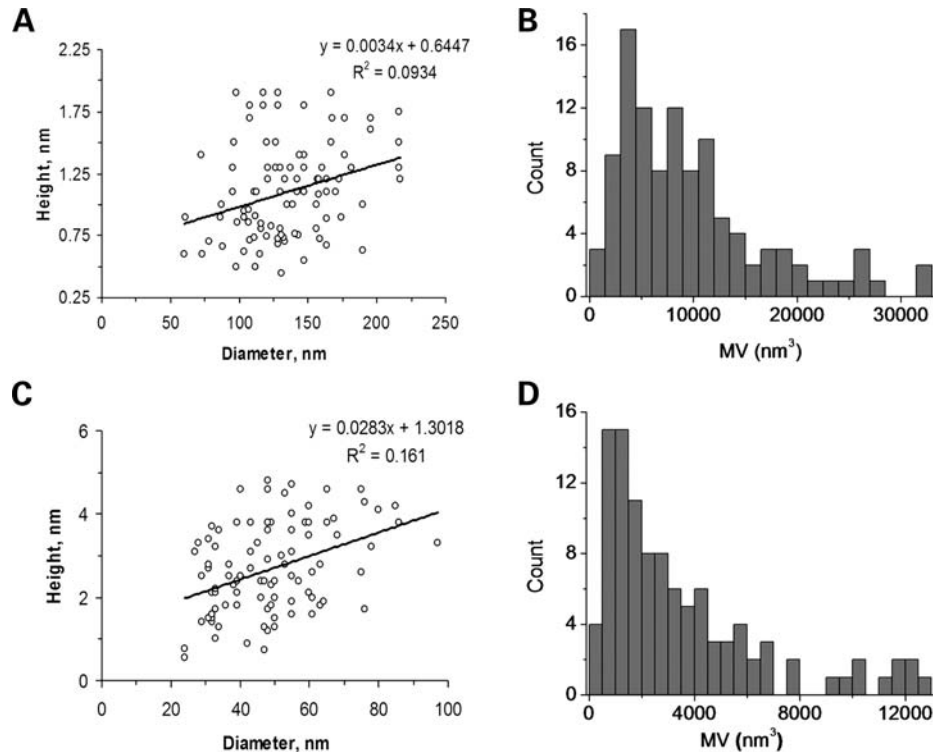


Figure 10. Distribution of the molecular volumes of PC2 and TRPC1 homomeric complexes. (A) The height–diameter relationship of PC2 ($n = 97$). Complexes with height higher than 2 nm were excluded from the analysis. A linear fitting showed no/weak linear correlation between height and diameter ($R^2 = 0.0934$). (B) Histogram of calculated molecular volume of PC2 molecular complexes. (C) Height–diameter relationship for TRPC1 ($n = 94$). Note the complexes with height higher than 5 nm were excluded from the analysis. A linear fitting also revealed no/weak correlation between height and diameter ($R^2 = 0.161$). (D) Histogram of calculated molecular volumes of TRPC1 complexes.

heteromultimer, resulting in the modulation of TRPC1 and PC2 properties. Our results, together with the published data, show the dramatic properties changes by heteromultimerization between PC2 and TRPC1.

AFM imaging of TRP (17) and other channels (37–39) has become recently available, which in combination with other high-resolution techniques such as cryo-electron microscopy (40,41) has rendered nanometer resolution of a number of channels. For example, Sato's group recently provided evidence for a bell-shaped structure of TRPM2 (40) and TRPC3 (41); Barrera *et al.* have also observed the tetrameric structure of TRPC1 (17) and trimeric structure of P2X2 (39) using AFM imaging. In those studies, however, as in others from the same group (37,38), the measurements, which are in strong agreement with their expected theoretical molecular volumes, are mostly consistent with a minimal volume occupied by the particles in solution. Because of the importance of membrane–channel interaction in determining the channel function, we studied the PC2/TRPC1 channel topology in lipid bilayers. The calculated molecular volumes of the PC2 or TRPC1 homomers in our study suggest much larger structures than their theoretical volumes, most likely the result of the conformational changes expected in the transmembrane structure of the channel protein in a lipid bilayer. When compared with more recent information on TRPC3 volume obtained from a molecular reconstruction of frozen hydrated samples by cryoelectron microscopy, for example, the value for TRPC3 is actually 10 times larger than the expected value from its molecular size. Using AFM, syncollin

can be observed as a monomer of molecular volume similar to its theoretical value as a naked protein on mica (42). After insertion of the protein into lipid layers, syncollin shows a doughnut shape consistent with a hexamer. The molecular volume of these structures is, on average, 706 nm³, which would render a monomer of 118 nm³, which is almost four times larger than the expected monomer (42). Recent AFM studies by Shahin *et al.* (43) showed that the C2A and C2B domains of synaptotagmin, an integral membrane protein of the synaptic vesicle, dramatically changed in size when imbedded in lipid bilayers. They showed that C2AB has a calculated molecular volume of 80 nm³, which is in agreement with the AFM measurement of 103 nm³ under 'naked' conditions. In lipid bilayers, however, much larger complexes of C2AB were observed. This report, which entails oligomerization (43), also shows that no particles in the 80 nm³ range are observed, suggesting that even the monomers are likely larger in the membrane. Thus, the calculated molecular volume of channels in lipids is generally larger than the expected theoretical value without lipids. Conversely, it is also possible that the channel insertion to the membrane also alters the lipid topological features and renders extrusions of membrane. Thus, the imaged channel structure in our AFM studies could include topological features from both channel proteins, and surrounding lipid bilayers. Our calculated channel diameters were much larger than those derived from the solution without lipids. Therefore, it is important to begin assessing the contribution of the natural environment, i.e. the lipid bilayer, to the conformational topology of transmembrane proteins such as ion channels. This information

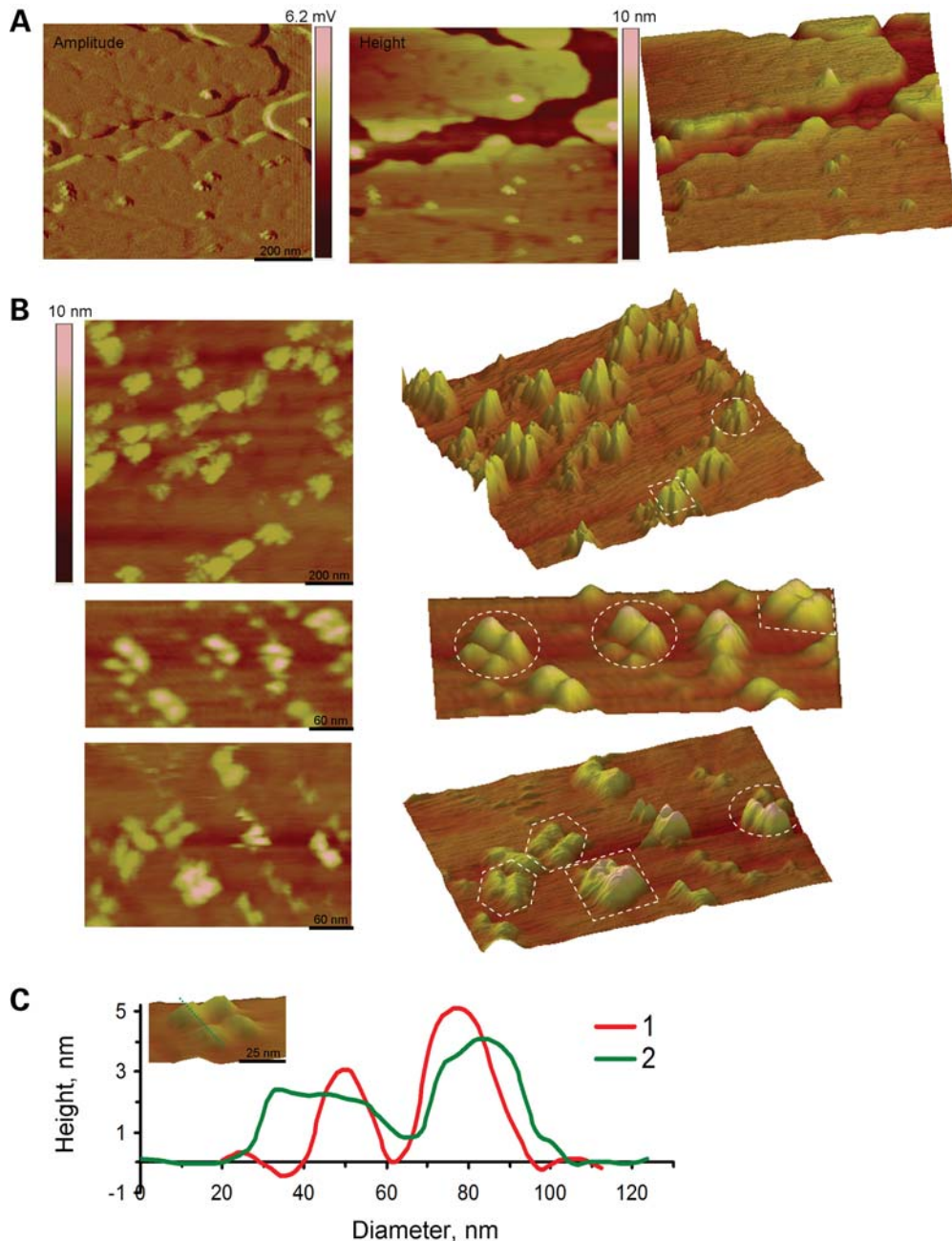


Figure 11. AFM imaging of PC2/TRPC1 hetero-complexes. (A) PC2/TRPC1 hetero-multimers were prepared by mixing (1:1) affinity purified PC2 and TRPC1 proteins, which were incorporated into liposomes. PC2/TRPC1-containing proteoliposomes were placed and flattened onto freshly cleaved mica in saline solution. The amplitude (Left), height (Middle) and the perspective (Right) images show the structure of both lipid and channel complexes at low magnification. (B) The height (Left) and perspective (Right) images at high magnification show that the hetero-multimeric channel complexes displayed lax, tetra-lobular shapes. These PC2/TRPC1 channel complexes had four contributing lobules of different height and a central indentation. The circles are examples of PC2/TRPC1 hetero-tetramers; the squares and hexagons highlight the TRPC1 homo-tetramer and PC2 homo-tetramer, respectively. (C) The height and diameter of the monomeric units in the PC2/TRPC1 channel complex could be easily identified in the cross-section histograms (insert, dashed lines). The higher peak correlates with TRPC1 monomers, whereas the lower peak with PC2 monomers.

is extremely relevant but has only recently begun to emerge. Previous studies from our laboratory (44) indicated that membrane-imbedded CFTR has a molecular volume larger than its theoretical one. Interestingly, the calculated volume of PC2 is much larger than that of the homomeric TRPC1. This suggests a larger intramolecular space in PC2 when compared with TRPC1, which may help explain the larger pore conductance

for PC2 (45) with respect to TRPC1. This phenomenon, which affects the electrophysiological and regulatory properties of the PC2/TRPC1 heteromeric complex, may also be reflected in the topological structure of the hetero-complex.

In summary, the data in this report indicate that both wild-type PC2 and TRPC1 form homotetramers, with distinct functional and regulatory properties, among which there

are the presence of four subconductance states in PC2. The AFM imaging of either of the respective homomers or the PC2/TRPC1 (2:2) hetero-complex is also consistent with a structural tetramer. This structural interaction is reflected in a functional correlation, namely the PC2/TRPC1 heteromers have functional properties, which are distinct from either homomeric structure alone. The AFM imaging also makes evident that the lipid bilayer plays an important role in the topological features of these channel proteins, and supports the contention that structural features in solution of transmembrane proteins are suitably explored in their natural environment. Functional diversity among TRP channels, and in particular the channel properties of PC2 and TRPC1 indeed depend on their mutual interactions, which affect both channels. This type of structural–functional correlation of heterologous oligomerization may be the basis of functional diversity among the TRP family members, and extend to other members, and thus other functions associated with these cellular sensors.

MATERIALS AND METHODS

Channel protein purification

PC2 protein was purified from HEK293T-S-PC2 cells over-expressing 6xHis-tagged PC2 protein. Ni-NTA spin columns (Qiagen, CA, USA) and a protocol for protein purification under native conditions were conducted as per manufacturer's recommendations. Briefly, cells were suspended and homogenized in lysis buffer, containing 50 mM NaH₂PO₄, 300 mM NaCl, 1% NP-40, 10 mM imidazole, supplemented with pepstatin, aprotinin, leupeptin and PMSF, pH 8.0. After centrifugation of cell lysate at 10 000g for 30 min, the supernatant was applied to a lysis buffer pre-equilibrated Ni-NTA column. After centrifugation at 700g for 2 min, the column was twice washed with wash buffer 1, containing 50 mM NaH₂PO₄, 300 mM NaCl, 1% NP-40, 30 mM imidazole and pepstatin, aprotinin, leupeptin and PMSF freshly, pH 8.0. This was followed by another two washes with wash buffer 2, containing 50 mM NaH₂PO₄, 300 mM NaCl, 2% NP-40, 25% glycerol, add pepstatin, aprotinin, leupeptin and PMSF, pH 8.0. PC2 was eluted from the column twice with elution buffer (50 mM NaH₂PO₄, 300 mM NaCl, 1% NP-40, 250 mM imidazole, and pepstatin, aprotinin, leupeptin and PMSF freshly, pH 8.0). TRPC1 preparation by flag affinity purification was conducted as follows. The purified flag-tagged protein was prepared from 293-S-TRPC1 cell lysates. Frozen cell pellets were added 1 ml Cellytic M reagent (Sigma), thawed out for 5 min and mixed well. The preparation was transferred to a 15 ml tube containing 4 ml Cellytic M reagent, and shake for another 15 min. The mixture was centrifuged and the supernatant of the cell lysate was loaded to the equilibrated column, and let flow through by gravity. The flow-through was collected, and the column was further washed with 5 ml (x1) of wash buffer. Proteins were eluted with 0.25 ml (x3) Flag peptide solution (200 ng/μl).

Western blot analysis of PC2

Western blot analyses were used to determine the size of the purified PC2 under both denaturing (SDS) and native

conditions. Purified PC2 was electrophoresed in native- and SDS–PAGE, and followed by electro-transfer to enhanced chemiluminescence (ECL) nitrocellulose membranes. PC2 was blotted using either a polyclonal anti-PC2 antibody (no. 96525, 1:1000 dilution) raised in rabbit to 44–62 amino acids of mouse PC2 intracellular N-terminal domain (27,46,47), or rabbit anti-polycystin-2 (Catalog no. 52-5217, 0.2 mg/ml Zymed, South San Francisco, CA, USA). Immunoblotting was detected with ECL system.

Proteoliposome preparation

PC2-containing proteoliposomes were prepared with a 7:3 mixture of L- α -phosphatidylcholine (PC, 10 mg/ml, Avanti Polar Lipids, Inc., AL) and 1-palmitoyl-2-oleoyl-Sn-Glycerol-3-phosphatidyl-ethanolamine (PE, 25 mg/ml, Avanti) to get 40 mg lipid mixture in n-decane, which were dried with nitrogen. The lipid mixture was added 4 ml of Na⁺-cholate buffer (25 mM Na⁺-cholate, 150 mM NaCl, 0.1 mM EDTA, 20 mM HEPES, pH 7.2) and sonicated in a water bath sonicator for 45 min. To prepare PC2 containing proteoliposomes, purified PC2 (1 μg/μl) was diluted to 1:1000. Diluted PC2 (1 μl) was added to 100 μl of lipid solution described above, mixed well with 0.2 μl of Na⁺-cholate and dialyzed against dialysis buffer (150 mM NaCl, 0.1 mM EDTA, 20 mM HEPES, pH 7.2) for 3 days at 4°C (with three changes of buffer). Similar procedures were followed for TRPC1 proteoliposome preparation. For the preparation of TRPC1/PC2 channel complexes, the ratio between PC2 and TRPC1 was 1:1.

Ion channel reconstitution

Lipid bilayers were formed with a mixture of synthetic phospholipids (Avanti Polar Lipids, Birmingham, AL, USA) in n-decane as reported (5). The lipid mixture was made of 1-palmitoyl-2-oleoyl phosphatidyl-choline and phosphatidyl-ethanolamine in a 7:3 ratio. The lipid solution (~20–25 mg/ml) was spread over the aperture of a polystyrene cuvette (CP13-150) of a bilayer chamber (model BCH-13, Warner Instruments Corp.). Both sides of the lipid bilayer were bathed with a solution containing MOPS-KOH, 10 mM and MES-KOH, 10 mM, pH 7.40, and 10–15 μM Ca²⁺. Both sides of the chamber had an initial, 15 mM K⁺ concentration, which was further supplemented to 150 mM in the *cis* side of the chamber to create a chemical gradient. Either membrane vesicles or proteoliposomes were added, to the *cis* side of the chamber. Wherever indicated, PC2 channel activity was determined from enriched hST membranes as reported (5).

Electrophysiological data acquisition and analysis

Electrical signals were recorded with a PC-501A patch clamp amplifier (Warner Instruments Corp.), using a 10 Gohm feedback resistor. Output signals were low-pass filtered at 1 kHz. Signals were displayed on an oscilloscope, and channel recordings were stored in a personal computer. Single-channel current tracings were further filtered for display purposes only. Unless otherwise stated, either pCLAMP Versions 5.5.1 or 10.0 (Axon Instruments, Foster City, CA, USA) were used

for data analysis. Sigmaplot Version 2.0 (Jandel Scientific, Corte Madera, CA, USA) was used for statistical analysis and graphics. Single-channel conductances were calculated as reported (5,26). Statistical significance was obtained by unpaired Student's *t*-test comparison of sample groups of similar size. Average data values were expressed as the mean \pm SEM (*n*) under each condition, where *n* represents the total number of experiments analyzed. Statistical significance was accepted at $P < 0.05$.

Atomic force microscopy

PC2 and TRPC1 channel complexes were imaged with either a Model 3000 atomic force microscope attached to a Nanoscope IIIa controller (Veeco Metrology, St Barbara, CA, USA), as reported (44,48), or a Model 3100 AFM attached to a NanoScope V controller, a kind loan from Veeco Metrology (see Acknowledgments). Samples were scanned with oxide-sharpened silicon-nitride tips (DNP-S, Veeco Metrology). Channel-containing proteoliposomes used for the lipid-bilayer reconstitution studies were used for AFM imaging studies. Proteoliposomes suspended in saline solution, containing 0.2 mM CaCl₂, 0.2 mM MgATP, 0.2 mM β -mercaptoethanol and 2 mM Tris-HCl, pH 7.15–7.25 were placed onto freshly cleaved mica disks. Proteoliposomes were flattened onto the mica surface by incubation for \sim 30 min at 37°C. Changes in saline pH were conducted by addition of HCl (1.0 N) to the solution in the scanning chamber.

Determination of molecular dimensions

The calculation of molecular dimensions for the various channel complexes was followed as originally reported by Schneider *et al.* (49). Briefly, multiple cross-sections of individual protein images by AFM were made and the mean diameters and heights of each unit were measured. As previously reported, we measured the diameter at half-maximal height of individual molecules, which sufficiently compensates for the artificially induced overestimation of the protein width. The molecular volume was calculated, after obtaining the dimensions of an individual protein (diameter and height), by treating the protein as a segment of a sphere. This calculation was done with the following equation, $V_m = (\pi h/6)(3r^2 + h^2)$, where V_m is the molecular volume, and *h* and *r* are the height and the radius of the protein, respectively. In addition, the molecular volume of the protein was calculated using the following equation: $V_c = (M_o/N_o)(V_1 + dV_2)$. Here, M_o is the molecular weight, N_o is Avogadro's number, and V_1 and V_2 are the partial specific volumes of the individual protein (0.74 cm³g⁻¹) and water (1 cm³g⁻¹), respectively. *d* is the extent of protein hydration (0.4 mol H₂O/mol protein) (49).

ACKNOWLEDGEMENTS

H.F.C. and his group wish to thank Dean Schmidt, Christopher Orsulak, Kim Reed, and John Thornton from Veeco Metrology (Sta. Barbara, CA, USA) for lending the Dimension

3100 atomic force microscope coupled to the NanoScope V controller, with which AFM imaging was made possible.

Conflict of Interest statement. None declared.

FUNDING

A.J.R. was partially funded by the PKD Foundation. J.Z. was supported by NIH DK53357 and DK074030.

REFERENCES

- Mochizuki, T., Wu, G., Hayashi, T., Xenophontos, S.L., Veldhuisen, B., Saris, J.J., Reynolds, D.M., Cai, Y., Gabow, P.A., Pierides, A. *et al.* (1996) PKD2, a gene for polycystic kidney disease that encodes an integral membrane protein. *Science*, **272**, 1339–1342.
- Montell, C. (2001) Physiology, phylogeny, and functions of the TRP superfamily of cation channels. *Sci. STKE*, **90**, RE1.
- Montell, C., Birnbaumer, L. and Flockerzi, V. (2002) The TRP channels, a remarkably functional family. *Cell*, **108**, 595–598.
- Montell, C., Birnbaumer, L., Flockerzi, V., Bindels, R.J., Bruford, E.A., Caterina, M.J., Clapham, D.E., Harteneck, C., Heller, S., Julius, D. *et al.* (2002) A unified nomenclature for the superfamily of TRP cation channels. *Mol. Cell*, **9**, 229–231.
- González-Perrett, S., Kim, K., Ibarra, C., Damiano, A.E., Zotta, E., Batelli, M., Harris, P.C., Reisin, I.L., Arnaout, M.A. and Cantiello, H.F. (2001) Polycystin-2, the protein mutated in autosomal dominant polycystic kidney disease (ADPKD), is a Ca²⁺-permeable nonselective cation channel. *Proc. Natl Acad. Sci. USA*, **98**, 1182–1187.
- Vassilev, P.M., Guo, L., Chen, X.Z., Segal, Y., Peng, J.B., Basora, N., Babakhanlou, H., Cruger, G., Kanazirska, M., Ye, C. *et al.* (2001) Polycystin-2 is a novel cation channel implicated in defective intracellular Ca²⁺ homeostasis in polycystic kidney disease. *Biochem. Biophys. Res. Commun.*, **282**, 341–350.
- Montalbetti, N., Li, Q., Timpanaro, G.A., González-Perrett, S., Dai, X.-Q., Chen, X.-Z. and Cantiello, H.F. (2005) Cytoskeletal regulation of calcium-permeable cation channels in the human syncytiotrophoblast. Role of gelsolin. *J. Physiol.*, **566**, 309–325.
- Nauli, S.M., Alenghat, F.J., Luo, Y., Williams, E., Vassilev, P., Li, X., Elia, A.E.H., Lu, W., Brown, E.M., Quinn, S.J., Ingber, D.E. and Zhou, J. (2003) Polycystins 1 and 2 mediate mechanosensation in the primary cilium of kidney cells. *Nat. Genet.*, **33**, 129–137.
- MacKinnon, R. (1991) Determination of the subunit stoichiometry of a voltage-activated potassium channel. *Nature*, **350**, 232–235.
- Catterall, W.A. (2000) Structure and regulation of voltage-gated Ca²⁺ channels. *Annu. Rev. Cell Dev. Biol.*, **16**, 521–555.
- Liu, D.T., Tibbs, S.A. and Siegelbaum, S.A. (1996) Subunit stoichiometry of cyclic nucleotide-gated channel and effects of subunit order on channel function. *Neuron*, **16**, 983–990.
- Xu, X.Z., Li, H.S., Guggino, W.B. and Montell, C. (1997) Coassembly of TRP and TRPL produces a distinct store-operated conductance. *Cell*, **89**, 1155–1164.
- Amiri, H., Schultz, G. and Schaefer, M. (2003) FRET-based analysis of TRPC subunit stoichiometry. *Cell Calcium*, **33**, 463–470.
- García-Sanz, N., Fernández-Carvajal, A., Morenilla-Palao, C., Planells-Cases, R., Fajardo-Sánchez, E., Fernández-Ballester, G. and Ferrer-Montiel, A. (2004) Identification of a tetramerization domain in the C terminus of the vanilloid receptor. *J. Neurosci.*, **24**, 5307–5314.
- Kedei, N., Szabo, T., Lile, J.D., Treanor, J.J., Olah, Z., Iadarola, M.J. and Blumberg, P.M. (2001) Analysis of the native quaternary structure of vanilloid receptor 1. *J. Biol. Chem.*, **276**, 28613–28619.
- Szallasi, A. and Blumberg, P.M. (1991) Molecular target size of the vanilloid (capsaicin) receptor in pig dorsal root ganglia. *Life Sci.*, **48**, 1863–1869.
- Barrera, N.P., Shaifa, Y., McFadzean, I., Ward, J.T.P., Henderson, R.M. and Edwardson, J.M. (2007) AFM imaging reveals the tetrameric structure of the TRPC1 channel. *Biochem. Biophys. Res. Commun.*, **358**, 1086–1090.
- Ferrer-Montiel, A., García-Martínez, C., Morenilla-Palao, C., García-Sanz, N., Fernández-Carvajal, A., Fernández-Ballester, G. and

- Planells-Cases, R. (2004) Molecular architecture of the vanilloid receptor. Insights for drug design. *Eur. J. Biochem.*, **271**, 1820–1826.
19. Johnson, J.P. Jr and Zagotta, W.N. (2001) Rotational movement during cyclic nucleotide-gated channel opening. *Nature*, **412**, 917–921.
 20. Rosenmund, C., Stern-Bach, Y. and Stevens, C.F. (1998) The tetrameric structure of a glutamate receptor channel. *Science*, **280**, 1596–1599.
 21. Delmas, P. (2004) Assembly and gating of TRPC channels in signalling microdomains. *Novartis Found. Symp.*, **258**, 75–97.
 22. Hoenderop, J.G., Voets, T., Hoefs, S., Weidema, F., Prenen, J., Nilius, B. and Bindels, R.J. (2003) Homo- and heterotetrameric architecture of the epithelial Ca²⁺ channels TRPV5 and TRPV6. *EMBO J.*, **22**, 776–785.
 23. Strübing, C., Krapivinsky, G., Krapivinsky, L. and Clapham, D.E. (2003) Formation of novel TRPC channels by complex subunit interactions in embryonic brain. *J. Biol. Chem.*, **278**, 39014–39019.
 24. Tsiokas, L., Arnould, T., Zhu, C., Kim, E., Walz, G. and Sukhatme, V.P. (1999) Specific association of the gene product of PKD2 with the TRPC1 channel. *Proc. Natl Acad. Sci. USA*, **96**, 3934–3939.
 25. Bai, C.-X., Giamarchi, A., Rodat-Despoix, L., Padilla, F., Downs, T., Tsiokas, L. and Delmas, P. (2008) Formation of a new receptor-operated channel by heteromeric assembly of TRPP2 and TRPC1 subunits. *EMBO Rep.*, **9**, 472–479.
 26. González-Perrett, S., Batelli, M., Kim, K., Essafi, M., Timpanaro, G., Montalbetti, N., Reisin, I.L., Arnaout, M.A. and Cantiello, H.F. (2002) Voltage dependence and pH regulation of human polycystin-2 mediated cation channel activity. *J. Biol. Chem.*, **277**, 24959–24966.
 27. Dedoussis, G.V.Z., Luo, Y., Starremans, P., Rossetti, S., Ramos, A.J., Cantiello, H.F., Katsareli, E., Ziroyannis, P., Lamnissou, K., Harris, P.C. and Zhou, J. (2008) Co-inheritance of a PKD1 mutation and homozygous PKD2 variant: a potential modifier in autosomal dominant polycystic kidney disease. *Eur. J. Clin. Invest.*, **38**, 180–190.
 28. Montalbetti, N., Li, Q., Wu, Y., Chen, X.-Z. and Cantiello, H.F. (2007) Polycystin-2 cation channel function in the human syncytiotrophoblast is regulated by microtubular structures. *J. Physiol.*, **579**, 717–728.
 29. Torres, V.E., Cai, Y., Chen, X., Wu, G.Q., Geng, L., Cleghom, K.A., Johnson, C.M. and Somlo, S. (2001) Vascular expression of polycystin-2. *J. Am. Soc. Nephrol.*, **12**, 1–9.
 30. Wu, Y., Dai, X.-Q., Li, Q., Chen, C.X., Cho, S., Hussain, Z., Montalbetti, N., Li, G., Glynne, R., Wang, S. *et al.* (2006) Kinesin-2 mediates physical and functional interactions between polycystin-2 and fibrocystin. *Hum. Mol. Genet.*, **15**, 3280–3292.
 31. Gaudet, R. (2008) TRP channels entering the structural era. *J. Physiol.*, **586**, 3565–3575.
 32. Lepage, P.K. and Boulay, G. (2007) Molecular determinants of TRP channel assembly. *Biochem. Soc. Transact.*, **35**, 81–83.
 33. Schindl, R. and Romanin, C. (2007) Assembly domains in TRP channels. *Biochem. Soc. Transact.*, **35**, 84–85.
 34. Becker, D., Müller, M., Leuner, K. and Jendrach, M. (2008) The C-terminal domain of TRPV4 is essential for plasma membrane localization. *Mol. Membr. Biol.*, **25**, 139–151.
 35. Celic, A., Petri, E.T., Demeler, B., Ehrlich, B.E. and Boggon, T.J. (2008) Domain mapping of the polycystin-2 C-terminal tail using de novo molecular modeling and biophysical analysis. *J. Biol. Chem.*, **283**, 28305–28312.
 36. Du, J., Sours-Brothers, S., Coleman, R., Ding, M., Graham, S., Kong, D.-H. and Ma, R. (2007) Canonical transient receptor potential 1 channel is involved in contractile function of glomerular mesangial cells. *J. Am. Soc. Nephrol.*, **18**, 1437–1445.
 37. Barrera, N.P., Henderson, R.M. and Edwardson, J.M. (2008) Determination of the architecture of ionotropic receptors using AFM imaging. Invited Review. *Pflügers Arch. Eur. J. Physiol.*, **456**, 199–209.
 38. Barrera, N.P., Herbert, P., Henderson, R.M., Martin, I.L. and Edwardson, J.M. (2005) Atomic force microscopy reveals the stoichiometry and subunit arrangement of 5-HT₃ receptors. *Proc. Natl Acad. Sci. USA*, **102**, 12595–12600.
 39. Barrera, N.P., Ormond, S.J., Henderson, R.M., Murrell-Lagnado, R.D. and Edwardson, J.M. (2005) Atomic force microscopy imaging demonstrates that P2X₂ receptors are trimers but that P2X₆ receptor subunits do not oligomerize. *J. Biol. Chem.*, **280**, 10759–10765.
 40. Maruyama, Y., Ogura, T., Mio, K., Kiyonaka, S., Kato, K., Mori, Y. and Sato, C. (2007) Three-dimensional reconstruction using transmission electron microscopy reveals a swollen, bell-shaped structure of transient receptor potential melastatin type 2 cation channel. *J. Biol. Chem.*, **282**, 36961–36970.
 41. Mio, K., Ogura, T., Hara, Y., Mori, Y. and Sato, C. (2005) The non-selective cation-permeable channel TRPC3 is a tetrahedron with a cap on the large cytoplasmic end. *Biochem. Biophys. Res. Commun.*, **333**, 768–777.
 42. Geisse, N.A., Wäsle, B., Saslowsky, D.E., Henderson, R.M. and Edardson, J.M. (2002) Syncoilin homo-oligomers associate with lipid bilayers in the form of doughnut-shaped structures. *J. Membr. Biol.*, **189**, 83–92.
 43. Shahin, V., Datta, D., Hui, E., Henderson, R.M., Chapman, E.R. and Edwardson, J.M. (2008) Synaptotagmin perturbs the structure of phospholipid bilayers. *Biochemistry*, **47**, 2134–2152.
 44. Chasan, B., Geisse, N.A., Pedatella, K., Wooster, D.G., Teintze, M., Carattino, M.D., Goldmann, W.H. and Cantiello, H.F. (2002) Evidence for direct interaction between actin and the cystic fibrosis transmembrane conductance regulator. *Eur. Biophys. J.*, **30**, 617–624.
 45. Anyatonwu, G.I. and Ehrlich, B.E. (2005) Organic cation permeation through the channel formed by polycystin-2. *J. Biol. Chem.*, **280**, 29488–29493.
 46. Li, Q., Montalbetti, N., Shen, P.Y., Dai, X.-Q., Cheeseman, C.I., Karpinski, E., Wu, G., Cantiello, H.F. and Chen, X.-Z. (2005) Alpha-actinin associates with polycystin-2 and regulates its channel activity. *Hum. Mol. Genet.*, **14**, 1587–1603.
 47. Luo, Y., Vassilev, P.M., Li, X., Kawanabe, Y. and Zhou, J. (2003) Native polycystin 2 functions as a plasma membrane Ca²⁺-permeable cation channel in renal epithelia. *Mol. Cell. Biol.*, **23**, 2600–2607.
 48. Raychowdhury, M.K., González-Perrett, S., Montalbetti, N., Timpanaro, G.A., Chasan, B., Goldmann, W.H., Stahl, S., Cooney, A., Goldin, E. and Cantiello, H.F. (2004) Molecular pathophysiology of mucopolipidosis type IV. pH dysregulation of the human mucolipin-1 cation channel. *Hum. Mol. Genet.*, **13**, 617–627.
 49. Schneider, S.W., Lärmer, J., Henderson, R.M. and Oberleithner, H. (1998) Molecular weights of individual proteins correlate with molecular volumes measured by atomic force microscopy. *Pflügers Arch.*, **435**, 362–367.